

# Fast and flexible range-separated models for atomistic machine learning

Philip Loche,<sup>1,2, a)</sup> Kevin K. Huguenin-Dumittan,<sup>1,2, a)</sup> Melika Honarmand,<sup>1,2</sup> Qianjun Xu,<sup>1,2</sup> Egor Rumiantsev,<sup>1,2</sup> Wei Bin How,<sup>1,2</sup> Marcel F. Langer,<sup>1,2</sup> and Michele Ceriotti<sup>1,2, b)</sup>

<sup>1)</sup>Laboratory of Computational Science and Modeling, IMX, École Polytechnique Fédérale de Lausanne, 1015 Lausanne, Switzerland

<sup>2)</sup>National Centre for Computational Design and Discovery of Novel Materials (MARVEL), École Polytechnique Fédérale de Lausanne, 1015 Lausanne, Switzerland

Most atomistic machine learning (ML) models rely on a locality ansatz, and decompose the energy into a sum of short-ranged, atom-centered contributions. This leads to clear limitations when trying to describe problems that are dominated by long-range physical effects – most notably electrostatics. Many approaches have been proposed to overcome these limitations, but efforts to make them efficient and widely available are hampered by the need to incorporate an ad hoc implementation of methods to treat long-range interactions. We develop a framework aiming to bring some of the established algorithms to evaluate non-bonded interactions – including Ewald summation, classical particle-mesh Ewald (PME), and particle-particle/particle-mesh (P3M) Ewald – into atomistic ML. We provide a reference implementation for *PyTorch* as well as an experimental one for *JAX*. Beyond Coulomb and more general long-range potentials, we introduce purified descriptors which disregard the immediate neighborhood of each atom, and are more suitable for general long-ranged ML applications. Our implementations are fast, feature-rich, and modular: They provide an accurate evaluation of physical long-range forces that can be used in the construction of (semi)empirical baseline potentials; they exploit the availability of automatic differentiation to seamlessly combine long-range models with conventional, local ML schemes; and they are sufficiently flexible to implement more complex architectures that use physical interactions as building blocks. We benchmark and demonstrate our *torch-pme* and *jax-pme* libraries to perform molecular dynamics simulations, to train range-separated ML potentials, and to evaluate long-range equivariant descriptors of atomic structures.

## I. INTRODUCTION

Machine learning (ML) has become essential in atomistic simulations, especially as a surrogate for quantum mechanical methods like density functional theory (DFT). Early works by Behler and Parrinello<sup>1</sup> and Bartók et al.<sup>2</sup> demonstrated that ML models are able to predict the energy and forces of an atomic structure at close to DFT accuracy with significantly reduced computational cost. Since then, the field has rapidly expanded in many directions: On one hand, various architectures including kernel-based approaches<sup>2–4</sup> and message-passing neural networks have emerged to further improve accuracy and efficiency<sup>5–9</sup>. Furthermore, beyond just the energy or other rotationally invariant target properties, the field has seen the rise of equivariant model architectures that can also handle tensorial target properties such as dipoles and polarizabilities<sup>10–12</sup>, the electron density<sup>13–15</sup>, the Hamiltonian operator<sup>16,17</sup> and many-particle wavefunctions<sup>18–20</sup>. Thanks to the mathematical field of representation theory, there is now a systematic understanding about how to incorporate any type of behavior under rotations in ML models<sup>21–23</sup>.

Despite these advancements, a persistent limitation in many of the ML models is the use of finite cutoff radii, which had been justified in terms of the “nearsightedness of electronic matter”<sup>24,25</sup>. While this allows for ef-

ficient methods with computational costs that scale linearly with the number of atoms, the trade-off is the introduction of systematic errors in scenarios where long-range interactions play a crucial role. For instance, electrostatic interactions from the direct Coulomb potential to induced multipolar interactions are critical in ionic and polar materials, affecting dielectric constants, phonon spectra, and structural stability<sup>26–28</sup>. Dispersion (van der Waals) forces are equally vital in layered materials, molecular crystals and interfaces, as they contribute to cohesion and adhesion energies<sup>29–31</sup>. Ignoring these interactions in ML models restricts their applicability.

This work presents libraries for the *PyTorch* and *JAX* frameworks that implement efficient methods for computing a family of long-range features as well as classical long-range energy corrections in an automatically differentiable manner. Due to the use of popular and flexible ML libraries, the features can easily be integrated into any pre-existing ML framework for invariant and equivariant target properties, with or without gradients.

In section II, we begin by providing an overview of the scientific background concerning algorithms for long-range electrostatics developed by the molecular dynamics (MD) community, as well as long-ranged ML methods. In section III, we discuss some of the specific technical choices and the core features of our implementation. In section IV, we demonstrate and benchmark in several different use cases our reference *torch-pme* implementation, providing also some comparisons with its more experimental *jax-pme* companion.

<sup>a)</sup>These two authors contributed equally.

<sup>b)</sup>Electronic mail: michele.ceriotti@epfl.ch

## II. BACKGROUND

Long-range interactions are not new to ML, and have in fact already been studied extensively since the outset of traditional atomistic simulations. Here we briefly summarize the key ideas.

### A. Notation and Conventions

We focus the discussion in this subsection on the Coulomb potential, and define the bare (or full) potential function

$$v(r) = \frac{1}{r} \quad (1)$$

for  $r \in (0, \infty)$ , even though the general setting of the problem applies to any pair potential, and we will discuss a few concrete cases of other  $1/r^p$ -type interactions. In a system of  $N$  atoms with positions  $\mathbf{r}_i \in \mathbb{R}^3$  and weights (charges)  $q_i$  for  $i = 1, \dots, N$ , the Coulomb potential  $V_i$  at the location of an atom  $i$  and the total energy  $E$  of the system can be defined as

$$V_i = \frac{1}{2} \sum_{j \neq i} q_j v(r_{ij}) \quad (2)$$

$$E = \sum_{i=1}^N q_i V_i, \quad (3)$$

where  $r_{ij} = \|\mathbf{r}_i - \mathbf{r}_j\|$  is the distance between atoms  $i$  and  $j$ , and we also include the factor of  $1/2$  to account for double-counting directly in the definition of  $V_i$ .

We can extend the atomic potentials to periodic systems by also including all interactions with periodic images of the atoms. Thus,

$$V_i = \frac{1}{2} \sum_{j=1}^N \sum_{\mathbf{l}}' q_j v(\|\mathbf{r}_i - \mathbf{r}_j - \mathbf{l}\|), \quad (4)$$

where  $\mathbf{l}$  runs over the lattice vectors of the periodic cell. The sum over  $j$  also includes  $i = j$  in the periodic case to take into account the interactions between atom  $i$  and its own periodic images. For this special case of  $i = j$ , the prime symbol in the second summation sign indicates that the term with  $\mathbf{l} = 0$  should be omitted.

While conceptually straight-forward, this definition of the potential in periodic space is problematic for the Coulomb potential since its slow decay makes the sum over  $\mathbf{l}$  conditionally convergent. A naive implementation (such as spherical summation) does not even converge in the first place<sup>32</sup>.

### B. Ewald Summation

The Ewald summation, published in 1921, remains a foundational method that effectively defines how to ex-

tend this computation to periodic systems<sup>33</sup>. The proposed solution is to perform a range-separation of the Coulomb potential: We write

$$v(r) = v_{\text{SR}}(r) + v_{\text{LR}}(r) \quad (5)$$

$$v_{\text{SR}}(r) = \frac{\text{erfc}\left(\frac{r}{\sqrt{2}\sigma}\right)}{r} \quad (6)$$

$$v_{\text{LR}}(r) = \frac{\text{erf}\left(\frac{r}{\sqrt{2}\sigma}\right)}{r}, \quad (7)$$

where  $\sigma$  is a ‘‘smearing’’ parameter that defines the range-separation and erf (erfc) is the (complementary) error function  $\text{erf}(x) = \frac{2}{\sqrt{\pi}} \int_0^x e^{-t^2} dt$  (and  $\text{erfc}(x) = 1 - \text{erf}(x)$ ). The first term  $v_{\text{SR}}$  contains the singularity of the Coulomb potential as  $r \rightarrow 0$  and decays quickly as  $r \rightarrow \infty$ . Thus, we call this the short-range part of the Coulomb potential.  $v_{\text{LR}}$  on the other hand decays as  $1/r$  as  $r \rightarrow \infty$  just like the Coulomb potential, but remains smooth and finite for  $r \rightarrow 0$ . We call it the long-range part of the Coulomb potential. The transition between the two happens roughly at  $r \approx \sigma$ . We will shortly discuss how to choose  $\sigma$  in practice.

Using this range-separation, the potential of atom  $i$  can be written as

$$V_i = \frac{1}{2} \sum_{j=1}^N \sum_{\mathbf{l}}' q_j v_{\text{SR}}(\|\mathbf{r}_i - \mathbf{r}_j - \mathbf{l}\|) \quad (8)$$

$$+ \frac{1}{2} \sum_{j=1}^N \sum_{\mathbf{l}}' q_j v_{\text{LR}}(\|\mathbf{r}_i - \mathbf{r}_j - \mathbf{l}\|). \quad (9)$$

Due to the fast decay of  $v_{\text{SR}}$ , the sum over  $j$  and  $\mathbf{l}$  in the first term converges quickly. We can thus efficiently implement it by introducing a cutoff radius  $r_{\text{cut}}$ , and only summing up the contributions up to this distance.

The second sum is still conditionally convergent, since  $v_{\text{LR}}$  contains the slowly decaying behavior of the Coulomb potential. However, since the singularity as  $r \rightarrow 0$  has been removed,  $v_{\text{LR}}$  is now a smooth function and hence has a quickly decaying Fourier transform given by

$$\hat{v}_{\text{LR}}(k) = \frac{4\pi}{k^2} e^{-\frac{1}{2}\sigma^2 k^2}; \quad (10)$$

$k = \|\mathbf{k}\|$  is the norm of the reciprocal space vector  $\mathbf{k}$ .

We can now use the Poisson summation formula, which allows us to convert a sum over a periodic lattice into a dual sum in reciprocal space. The details on the used conventions for Fourier transforms and a proof of the Poisson summation formula for the convenience of readers can be found in section S1 of the supporting information. The

final result for the potential of atom  $i$  is

$$V_i = V_{i,\text{SR}} + V_{i,\text{LR}} + V_{i,\text{charge}} + V_{i,\text{self}} \quad (11)$$

$$V_{i,\text{SR}} = \frac{1}{2} \sum_{j=1}^N \sum_{\mathbf{l}}' q_j v_{\text{SR}}(\|\mathbf{r}_i - \mathbf{r}_j - \mathbf{l}\|) \quad (12)$$

$$V_{i,\text{LR}} = \frac{1}{2\Omega} \sum_{j=1}^N \sum_{\mathbf{k} \neq 0} q_j \hat{v}_{\text{LR}}(\mathbf{k}) e^{i\mathbf{k}(\mathbf{r}_i - \mathbf{r}_j)} \quad (13)$$

$$V_{i,\text{self}} = -\frac{1}{2} q_i \sqrt{\frac{2}{\pi}} \frac{1}{\sigma} \quad (14)$$

$$V_{i,\text{charge}} = -\frac{1}{2} \frac{\pi \sigma^2 q_i Q}{\Omega}, \quad (15)$$

where  $\Omega$  is the volume of the unit cell, the sum over  $\mathbf{k}$  is a sum over all nonzero reciprocal space lattice vectors and  $Q = \sum_i q_i$  is the total charge of all atoms in the unit cell. We have kept the overall factor of  $1/2$  that arises from double counting at the front for better comparison with results from some authors which omit this factor. The extra term  $V_{i,\text{charge}}$  is required to enforce charge neutrality, a requirement of the method. If the provided charges  $q_i$  do not lead to a charge-neutral cell, a homogeneous background charge is added to the system to ensure overall neutrality in the unit cell. The term is then the interaction between an atom and this background charge.  $V_{i,\text{self}} = \frac{1}{2} q_i v_{\text{LR}}(0)$  is the self-term which compensates the interaction of an atom with itself via  $v_{\text{LR}}$ , which is an artifact of the reciprocal space sum.

Due to the fast decay of  $\hat{v}_{\text{LR}}(k)$  as  $k \rightarrow \infty$ , the long-range sum can now also be computed efficiently by choosing a cutoff  $k_{\text{cut}}$  and truncating the sum by only including terms for which  $k \leq k_{\text{cut}}$ . The naive Ewald algorithm has a computational cost scaling quadratically with the number of atoms,  $\mathcal{O}(N^2)$ , while optimizations – letting  $r_{\text{cut}}$  scale with the size of the unit cell – can bring the exponent in the scaling down to  $\mathcal{O}(N^{3/2})$ <sup>34</sup>.

### C. Generalization to Arbitrary Exponents

Beyond the Coulomb potential, this work has been extended a few decades later to other interactions, including more general power-law potentials  $v(r) = 1/r^p$  with an interaction exponent  $p > 0$ <sup>35–38</sup>. The Coulomb interaction corresponds to  $p = 1$ , while dispersion corresponds to  $p = 6$ . Summarizing their results using our conventions and notations, the range-separation  $v = v_{\text{SR}} + v_{\text{LR}}$  is performed using

$$v_{\text{SR}}(r) = \frac{1}{\Gamma(\frac{p}{2})} \frac{\Gamma(\frac{p}{2}, \frac{r^2}{2\sigma^2})}{r^p} \quad (16)$$

$$v_{\text{LR}}(r) = \frac{1}{\Gamma(\frac{p}{2})} \frac{\gamma(\frac{p}{2}, \frac{r^2}{2\sigma^2})}{r^p} \quad (17)$$

$$\hat{v}_{\text{LR}}(k) = \frac{\pi^{3/2} 2^{3-p} \Gamma(\frac{3-p}{2}, \frac{1}{2}\sigma^2 k^2)}{\Gamma(\frac{p}{2}) k^{3-p}}, \quad (18)$$

where  $\Gamma(x) = \int_0^\infty t^{x-1} e^{-t} dt$  is the (complete) Gamma function,  $\Gamma(a, x) = \int_x^\infty t^{x-1} e^{-t} dt$  is the upper incomplete Gamma function and  $\gamma(a, x) = \Gamma(a) - \Gamma(a, x)$  the lower incomplete Gamma function. Up to a prefactor, we see that the functional form of  $\hat{v}_{\text{LR}}$  is identical to  $v_{\text{SR}}$ , the difference being that  $r/\sigma$  gets replaced by  $\sigma k$  and  $p$  by  $3-p$ . This high degree of symmetry is one reason that makes this particular choice of  $v_{\text{SR}}$  efficient. Note that some packages like *PyTorch* implement the incomplete Gamma functions with an extra prefactor.

To get the atomic potentials, the decomposition

$$V_i = V_{i,\text{SR}} + V_{i,\text{LR}} + V_{i,\text{charge}} + V_{i,\text{self}} \quad (19)$$

is still valid, where the first two terms are computed using the identical method but using the generalized expressions for  $v_{\text{SR}}$  and  $\hat{v}_{\text{LR}}$ , while

$$V_{i,\text{self}} = -\frac{q_i}{2} \frac{1}{(2\sigma^2)^{\frac{p}{2}} \Gamma(\frac{p}{2} + 1)} \quad (20)$$

$$V_{i,\text{charge}} = -\frac{q_i}{2} \frac{\pi^{\frac{3}{2}} (2\sigma^2)^{\frac{3-p}{2}} Q}{(3-p) \Gamma(p/2) \Omega}. \quad (21)$$

### D. Mesh-Based Approaches

The Ewald sum provided the first absolutely convergent formulation for the potential in a periodic system, and remains important to this day. It suffers, however, from a relatively inefficient computational scaling with the number of atoms. Thus, many algorithms have been developed to significantly reduce the computational cost of the Ewald sum, enabling the use of long-range methods for the simulation of large-scale systems. The most important family for this work consists of the particle-mesh methods, such as particle-particle particle-mesh (P3M) which was published first<sup>39,40</sup>, the original particle mesh Ewald (PME)<sup>41</sup> and its extension called smooth PME (SPME)<sup>42</sup>. These are based on the fast Fourier transform (FFT), and bring the asymptotic scaling of the computational cost down to  $\mathcal{O}(N \log N)$ . Due to the use of Fourier transforms, they assume periodicity in the system just like the Ewald sum, but can also be used for aperiodic systems with some care and modifications.

The key idea is that the two sums appearing in Equation 13 can “almost” be interpreted as discrete Fourier transforms: We can in fact break down the computation of  $V_{i,\text{LR}}$  into the two sums

$$\hat{q}(\mathbf{k}) = \sum_{j=1}^N q_j e^{-i\mathbf{k}\mathbf{r}_j} \quad (22)$$

$$V_{i,\text{LR}} = \sum_{\mathbf{k} \neq 0} \hat{q}(\mathbf{k}) \hat{v}_{\text{LR}}(k) e^{i\mathbf{k}\mathbf{r}_i}. \quad (23)$$

Both Equation 22 and Equation 23 look quite similar to Fourier transforms, but with one key difference: The positions  $\mathbf{r}_i$  and  $\mathbf{r}_j$  are in general not equally spaced.

Thus, despite the apparent similarity, these cannot directly be computed using algorithms for the discrete Fourier transform.

The similarity however motivates the following trick: In order to use the efficient FFT algorithm, we can interpolate the weights  $q_i$  onto an equally-spaced mesh. This generates an effective (charge) density  $\rho$  that is only defined on the mesh. While this changes the position of the particles, and hence introduces discretization errors, the regular nature of the particle positions now allows us to compute the appropriately modified versions of both Equation 22 and Equation 23 efficiently using three-dimensional FFT. The computational cost typically scales as  $\mathcal{O}(N \log N)$ , assuming a fixed mesh spacing and that the system volume is proportional to the number of atoms. This general description and scaling is common to all mesh-based methods.

The PME, P3M and SPME methods simply differ in (1) the choice of interpolation scheme between the particle positions and the mesh, (2) the particular choice of  $\hat{v}_{\text{LR}}$  that is used in Equation 23, and (3) the method to perform the differentiation to compute the electric field or forces. We briefly summarize the first two key distinguishing points for PME and P3M, as these are particularly relevant for this work. Deserno and Holm<sup>40</sup> provide a more detailed discussion for each of these.

The original version of PME<sup>41</sup> is the simplest for both (1) and (2). The interpolation is performed using (piecewise) Lagrange interpolation, a well-known technique in numerical analysis<sup>43</sup>. Furthermore,  $\hat{v}_{\text{LR}}$  remains the same as for the Ewald summation, Equation 10 for Coulomb and Equation 18 for the general case. It can in fact be shown that for this choice of  $\hat{v}_{\text{LR}}$ , the Lagrange interpolation scheme is optimal regarding the discretization errors arising due to the mesh<sup>40</sup>.

This is the simplest of the three variants to implement, and therefore serves as a convenient testing ground for new implementations. One key downside, however, is that the interpolation scheme leads to non-smooth behavior or even discontinuities, making the method less suitable for our approach that fully exploits the autodifferentiable nature of *PyTorch* and *JAX*. The authors of PME have in fact addressed this issue by presenting the SPME algorithm just two years after the original version<sup>42</sup>.

The P3M algorithm, despite being more complex than the original PME, was historically presented first. It is widely used due to its superior accuracy<sup>40</sup>. The key idea is that in a periodic system, the effective Coulomb potential is different than in vacuum due to the periodic neighbors. This is what suggests a modification of  $\hat{v}_{\text{LR}}$  by taking into account the periodic cell. Since the crystal lattice breaks rotation symmetry,  $\hat{v}_{\text{LR}}(\mathbf{k})$  no longer is spherically symmetric and now depends on the three-dimensional vector  $\mathbf{k}$  rather than just its norm  $k$ . In practice,  $\hat{v}_{\text{LR}}$  is obtained by minimizing an estimated force error due to discretization. P3M further uses a custom interpolation scheme that is obtained from requiring a

smoother interpolation. The combination of the interpolation scheme and optimized  $\hat{v}_{\text{LR}}$  makes P3M more accurate, and hence a popular choice despite its higher complexity compared to naive PME.

Beyond the mesh-based ones, many other algorithms have been developed to efficiently compute electrostatic interactions, including the fast multipole method that was the first linearly scaling  $\mathcal{O}(N)$  method for electrostatics<sup>44,45</sup>. Despite the better asymptotic scaling, the larger prefactor typically makes the particle-mesh methods more suitable for system sizes relevant to our field, which is why we focus on the latter in this work.

## E. Long-Range ML Models

Inspired by these developments for long-range interactions in the last century, it has become increasingly popular for ML models in atomistic modeling to incorporate long-range corrections as well. In fact, one of the founding works by Bartók et al.<sup>2</sup> already included an explicit dispersion term in the prediction of the energy for GaAs structures. A similar strategy has been used by many subsequent works<sup>46–50</sup>, in which the energy and optionally the forces of a structure are predicted as the sum of a more sophisticated ML part, and an explicit long-range term of the form  $1/r^p$ . Typically, each chemical species is assigned a fixed weight (or charge in the case of Coulomb interactions) in these interactions. This makes it simple to train the models, and has the advantage that it can be combined with essentially any model architecture.

In the last five years, the field has also seen the rise of more sophisticated approaches going beyond simple point charge models to handle more complex datasets. One extension is to make the particle weights or charges themselves dependent on the atomic environments<sup>51,52</sup>, and to learn this relationship directly from the data. Alternatively, it has been proposed to learn the Wannier centers<sup>53,54</sup>. This allows the center of the electron charge to be different from the positively charged ion, naturally capturing dipolar effects. Alternatively, it is possible to learn electronegativities rather than the charges, and to compute the charges from a subsequent charge equilibration scheme<sup>55–58</sup>. This approach has the advantage that the final charges can depend on atoms beyond a local cutoff, and hence can capture nonlocal charge transfer. A general property of these methods is that they are most naturally designed to have the energy (and forces) as the target property. This specialization makes the methods very powerful for this task, but less suitable to other target properties. In addition, the original implementation lacked efficiency and scalability, but this was recently resolved by also using a mesh paradigm<sup>58</sup> improving the scaling significantly.

While these approaches work well to incorporate the energy corrections, there is one common deficit: The fact that the Coulomb potential (or more general power-laws) at the position of an atom, despite being a long-range

property that also depends on atoms that are far away, is still primarily determined by neighbor atoms that are close by. This makes such potentials ill-suited to be used as a truly general long-range descriptor.

An alternative approach, developed by some of the authors in this work, emphasizes constructing general equivariant features that encode long-range on top of short-range information, rather than focusing directly on the energy as a target property<sup>59–61</sup>. These long-distance equivariant (LODE) features can be applied in various ML models to predict a range of target properties, from scalar invariants to higher-order equivariants. While prior studies have primarily explored the method’s capabilities, the implementation used an Ewald-like summation approach<sup>61</sup>, leading to an  $\mathcal{O}(N^2)$  scaling. This quadratic scaling limits the method’s applicability to larger systems. As already mentioned, LODE in its original formulation is not a range-separated descriptor, but contains all short-range and long-range contributions of a system, which limits its descriptive power. However, this can be resolved by constructing a modification of the original formulation that only includes long-range information<sup>61,62</sup>. In addition, recently there is strong evidence<sup>58,63,64</sup> that using a full spherical expansion of the potential is not necessary to describe long-range effects in machine learning models, but so far there is no rigorous investigation of these observations.

### III. METHOD

Our primary goal is to design a library to compute long-range interactions that can be easily integrated with existing short-range architectures, essentially providing an easy-to-use framework to build range separated models for atomistic machine learning. To this end, our reference *torch-pme* library provides

1. A modular implementation of range-separated potentials,
2. Full integration with *PyTorch*, featuring differentiable and learnable parameters,
3. Efficient particle-mesh-based computation with automatic hyperparameter tuning,
4. Pure long-range descriptors, free of noisy short-range contributions,
5. Support for arbitrary invariant and equivariant features and ML architectures.

We discuss these features in general terms, without focusing too much on the specific API, because similar ideas can be readily implemented with other ML frameworks, as we are currently doing with an experimental *jax-pme* library.

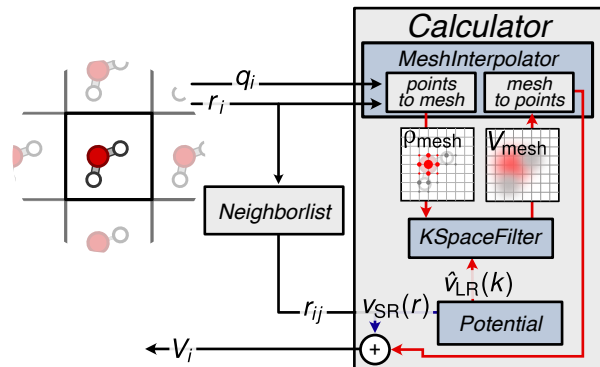


Figure 1. A schematic representation of the main building blocks that are contained inside a *Calculator* of a range-separated architecture, that combines an evaluation of the short-range part of the potential  $v_{\text{SR}}(r)$  based on local interatomic distance information with the evaluation of the long-range part  $v_{\text{LR}}(k)$  using grids via a *MeshInterpolator* and a *KSpaceFilter*.

#### A. A modular implementation of range-separated models

As discussed in section II, the key concept underlying all efficient methods to model long-range interactions is to split the calculation of the pair interactions between two particles into a short and long-range parts, i.e.  $v(r) = v_{\text{SR}}(r) + v_{\text{LR}}(r)$ . The short-range part, that decays to (effectively) zero beyond a set cutoff distance  $r_{\text{cut}}$  is computed summing over the neighbors of each particle. The required pair distances  $r_{ij}$  for the short range part have to be calculated with an external *Neighborlist* code, which is also needed for any short-range component of a ML model, and can be easily precomputed during training. The long-range part is computed in  $k$ -space, based on its Fourier transform  $\hat{v}_{\text{LR}}(k)$  and requires the absolute position vectors  $\mathbf{r}_i$  as well as the particle weights  $q_i$  (that correspond to charges for an electrostatic potential). Furthermore, the methods with an efficient scaling in the asymptotic limit, such as PME or P3M, convert the particle-based description into a smooth particle density, discretizing it on a real-space mesh, and using fast Fourier transforms to perform a Fourier convolution.

These ingredients can be used for more general tasks than computing explicitly physical interatomic potentials. To make this possible, the implementation we propose follows a modular design, in which a *Potential* class exposes methods to compute  $v(r)$ ,  $v_{\text{SR}}(r)$ ,  $v_{\text{LR}}(r)$ ,  $\hat{v}_{\text{LR}}(k)$ ; a *MeshInterpolator* converts particle positions  $\mathbf{r}_i$  and pseudo-charges  $q_i$  into a density mesh, and vice-versa interpolates a scalar field defined on the mesh at arbitrary positions; a *KSpaceFilter* performs the Fourier-domain convolution.

These elements can be combined in a *Calculator* object that applies one of the classical algorithms to compute long-range interactions, evaluating the potential at the atomic positions,  $V_i = V(\mathbf{r}_i)$  (see Figure 1). How-

ever, the same modular components can also be used in more complex ways. For example, users can compute descriptors based on the local potential in a neighborhood around each atom, such as LODE<sup>59,61</sup> features (section IV E). As long as all components are implemented within an auto-differentiable framework, both the base calculators and any custom architecture allows to easily evaluate derivatives of the predictions with respect to particle coordinates, cell matrix, and model parameters.

## B. Fully Differentiable and Learnable Framework

The integration of long-range calculators with ML libraries built around automatic evaluation of gradients enables seamless differentiation and parameter optimization, making them easy to combine with any *PyTorch* and *JAX*-based ML model. This includes optimizing parameters such as the particle weights  $q_i$  and even the type of interaction itself by e.g. parametrizing the interaction as  $v(r) = w_1/r + w_2/r^2 + w_3/r^3$ , where  $w_1$ ,  $w_2$ , and  $w_3$  are learnable. This flexibility is illustrated for both simple toy systems (section IV C) and complex model architectures (section IV D). *PyTorch* uses automatic differentiation to efficiently obtain gradients of target properties. This makes the implementation of models that learn both the energies and forces effortless.

## C. Hyperparameter Tuning

Range separated calculations like Ewald and its mesh-based variants require careful distribution of the computational load between the real-space and the Fourier space contributions. This is relevant both for computational performance and correctness; poor choices of parameters can lead to severe errors of the potential and the forces. This includes parameters like the mesh spacing and the real-space interaction cutoff. Using *PyTorch*'s optimization capabilities, the package comes with a built-in tuning functionality that simplifies the process for non-experts for the Coulomb potential based on known error estimates for the force error  $\mathcal{E}_F$ <sup>65,66</sup>. To this end, the relevant parameters, which we call  $\theta$ , are optimized to minimize the estimated absolute convergence errors  $\mathcal{E}_F(\theta)$  in the forces below a target accuracy  $\epsilon_{\text{target}}$ .

The accuracy can be set by the user, with some default suggestions. The minimization is performed using gradient descent starting from an initial guess  $\theta_0$  obtained from heuristics. The force error estimate  $\mathcal{E}$  also depends on the algorithm used, as it is different for Ewald summation, PME, and P3M. Further details and the concrete mathematical expressions can be found in section S2 of the supporting information. Benchmark results in section IV A demonstrate and compare the obtained accuracy with the desired value  $\epsilon_{\text{target}}$ , as well as the resulting speed.

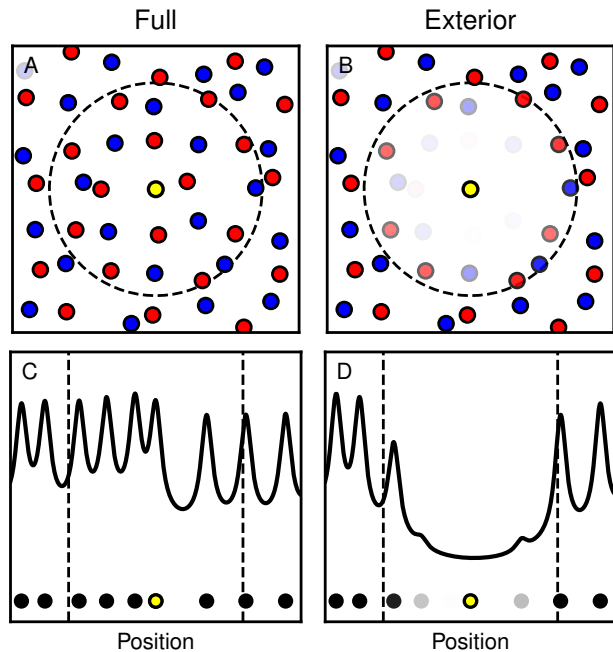


Figure 2. Schematic representation of the atoms contributing to the full potential (A) and exterior potential features (B). Each circle represents an atom that contributes to the potential of the center atom shown in yellow, with the cutoff circle shown as a dotted line. In the latter case, the contribution of interior atoms is gradually turned on as their distance approaches the cutoff. Panels (C) and (D) show a one-dimensional example, where the vertical axis now shows the (smeared) Coulomb potential generated by the atoms. The sharp drop of the potential curve after removing the interior contributions shows how the electrostatic potential around an atom is mostly dominated by its immediate neighbors, despite the long-range nature of the Coulomb potential.

## D. Exterior potential features

When computing physical interactions, the potential generated on a central atom  $i$  by a set of  $N$  atoms with weights  $q_j$  at distances  $r_{ij}$  can be expressed as

$$V_i^{\text{full}} = \frac{1}{2} \sum_{j \neq i} q_j v(r_{ij}), \quad (24)$$

where  $p > 0$  is the exponent associated with the interaction, e.g.,  $p = 1$  for Coulomb and  $p = 6$  for dispersion forces. The sum can be performed explicitly for a finite system, while a more general definition is necessary in the periodic case, as discussed in section II. This atom-centered potential contains information on the position of atoms in the far-field. It is however not an ideal descriptor of long-range interactions: Despite being physically motivated, it also contains unwanted short-range effects from particles in the vicinity of the atom of interest.

In practice, short-ranged ML models are already excellent at extracting short-ranged information from neighbor atoms up to a cutoff radius  $r_{\text{cut}} > 0$ . To real-

ize “range-separated”, multi-scale models, it is therefore preferable to obtain purely long-ranged features. To this effect one can introduce “exterior potential features” (EPFs)

$$V_i^{\text{ext}} = \frac{1}{2} \sum_{r_{ij}} q_j f_{\text{trans}}(r_{ij}) v(r_{ij}) \quad (25)$$

$$\approx \frac{1}{2} \sum_{r_{ij} > r_{\text{cut}}} q_j v(r_{ij}) \quad (26)$$

that eliminate the contributions from atoms within the cutoff, that are already well-modeled by the short-range part of the model (see Figure 2A and B). The transition function  $f_{\text{trans}}$  essentially eliminates the contribution from interior atoms, but does so in a smooth way to ensure the differentiability of the features as atoms leave or enter the interior region. It is explicitly given by

$$f_{\text{trans}}(r) = \begin{cases} \frac{1 - \cos\left(\frac{r^n}{r_{\text{cut}}^n}\right)}{2} & r < r_{\text{cut}} \\ 1 & r \geq r_{\text{cut}}, \end{cases} \quad (27)$$

with some exponent  $n$  that controls how quickly the contributions of the interior atoms vanishes as they approach the cutoff.

To illustrate the benefit of the exterior variant, consider the electrostatic (Coulomb) potential generated by a one-dimensional chain of Gaussian charge distributions. Figure 2C shows the full variant, while D corresponds to the exterior variant. The stark difference in the two curves around the location of the center atom  $i$  shows that even for the very slowly decaying Coulomb potential, the potential around an atom is most strongly influenced by the immediate neighbors. If the goal is to obtain long-ranged features to combine them with a short-ranged model, we can see that the exterior variant offers a clean signal, while the full potential features are contaminated by the redundant short-range contributions. *torch-pme* provides an implementation of this idea, similar to a construction that has already been used in our previous work<sup>61</sup>. This is a key difference with approaches that are based on the explicit modeling of physical interactions.

### E. Implementing range-separated ML architectures

There are two main approaches one can take to incorporate long-range terms in an ML architecture. One involves re-purposing traditional range-separated calculators to evaluate potential-like values at the atomic positions, and combine them with short-range model architectures to compute short-range interactions, atomic pseudo-charges, or arbitrary non-linear combinations of local descriptors and atom-centered potentials. Given that the atom-centered potential values are (in the limit of a converged mesh) translationally and rotationally invariant, this approach can be easily applied to make in-

variant or equivariant predictions. In addition, a full separation of a short and long-range model allows that with an appropriate architecture one can safely use multiple time stepping schemes to further reduce the overhead stemming from the long-range evaluation<sup>67,68</sup>.

The second approach exploits the fact that mesh-based range-separated calculators return the potential values on a grid that covers the entire system. This makes it possible to evaluate equivariant atom-centered features (along the lines of the LODE framework<sup>59,61</sup>) and combine them with equivariant local descriptors within an equivariant architecture.

Even though the latter approach is more general (and can be used, for instance, to describe many-body non-covalent interactions<sup>61</sup>) analytical considerations indicate that the most important information on long-range pair interactions is contained in the invariant part of the descriptors (see also the SI for a more thorough discussion). For this reason, the core components of the library we developed focus on the evaluation of invariant features, which facilitate constructing fast, flexible and streamlined range-separated models. Nevertheless, the *torch-pme* API does allow to evaluate fully equivariant LODE features quite easily, as we show in section IV E.

## IV. BENCHMARKS AND MODEL ARCHITECTURES

Having discussed some of the general principles, and the overall structure of our implementation, we now move on to discuss some practical examples and benchmarks. If not stated otherwise, all presented results are obtained using the *torch-pme* implementation in single precision. In section IV A we begin by presenting benchmarks on the speed and accuracy of the implementation. To further validate the correct behavior of the “full potential” for more complex systems, section IV B presents MD trajectories in which our algorithms have been used to compute the electrostatic forces via a LAMMPS interface, and compare the results against LAMMPS’s own P3M implementation. In order to showcase the flexibility of *torch-pme*, section IV C illustrates how our implementations easily allows learning different interaction types and charges. Beyond these toy systems, section IV D provides an example of a more involved model architecture, and compares the results to previous work. Finally, section IV E discusses how to use the building blocks of *torch-pme* can be used to evaluate more complicated equivariant features.

### A. Benchmark: Speed and Accuracy

We begin by discussing the results on the automatic hyperparameter tuning, as this also determines the parameters used for the remaining tests on speed and accuracy. For many simple crystal structures, lattice energies assuming purely electrostatic interactions and ideal

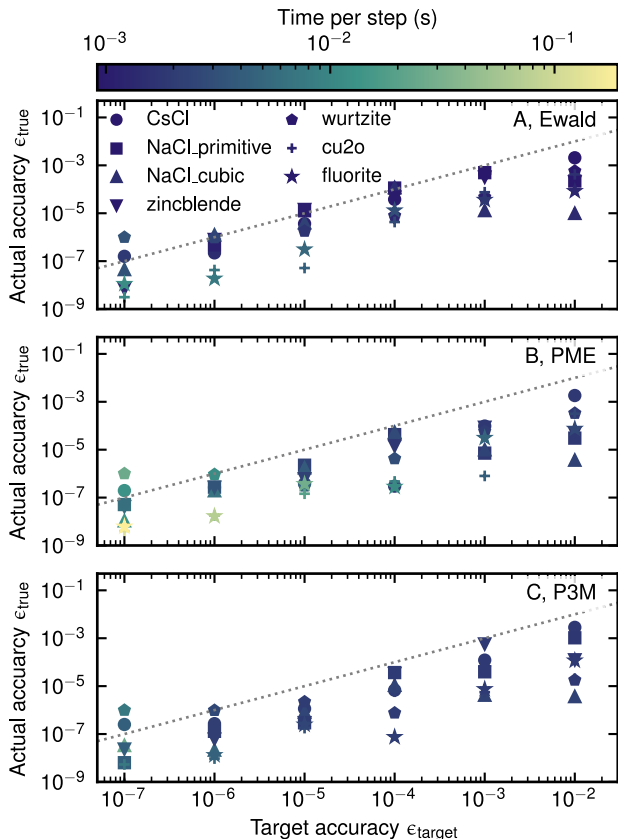


Figure 3. Empirical versus target accuracy after tuning calculator parameters for different replicated crystal structures and long-range methods. Panels show results for Ewald (A), PME (B) and P3M (C). Each crystal was replicated to reach from its initial unit cell structure until it contains at least 1000 atoms. Different symbols represent different crystals. The true target accuracies are obtained from the Madelung constants which were taken from 69 and 70.

formal charges (commonly referred to as Madelung constants) are known and tabulated with great accuracy. We define the actual (relative) accuracy as

$$\epsilon_{\text{true}} = \frac{|E_{\text{actual}} - E_{\text{reference}}|}{E_{\text{reference}}}, \quad (28)$$

where  $E_{\text{actual}}$  is the obtained energy and  $E_{\text{reference}}$  are the tabulated reference energies. Figure 3 show the relative accuracy of the predicted energies after tuning the parameters for the Ewald summation and the mesh calculators in double precision for a given desired accuracy  $\epsilon_{\text{desired}} = \Delta F/F_{qq}$ , where  $F_{qq}$  is the constant force created by two elementary charges at separated by 1 Angstrom to convert absolute errors into an estimated relative error as is also done in LAMMPS. We compute and show results for crystal structures that were replicated 8 times in each direction, so that each structure contains at least 1000 atoms. For each structure, the actual accuracy  $\epsilon_{\text{true}}$  is plotted against the desired accuracy

$\epsilon_{\text{target}}$ , meaning that ideally, all points should lie below the black dotted line defined by  $\epsilon_{\text{true}} = \epsilon_{\text{desired}}$ . Points are color-coded according to the computational cost of the calculation performed on a single AMD EPYC 9334 CPU and one NVIDIA H100 SXM5 GPU. In section S2 of the supplementary material we show figures presenting the actual relationship between the accuracy and the computational cost for the different methods and precisions. As expected, we find that tighter parameters lead to higher computational cost. In Figure S1 in the supplementary material we show the same results for single precision where we find that the accuracy saturates around  $10^{-6}$  for Ewald summation and  $10^{-5}$  for the mesh calculators.

For a diverse dataset containing structures with different numbers of atoms, we recommend tuning the parameters on the system with the largest cell and largest number of particles. A more detailed discussion of these considerations, as well as more detailed plots on the auto-tuning of the parameters and the convergence can be found in the supporting information.

Accuracy is only one aspect of successful numerical software. In Figure 4, we demonstrate that our implementations are also competitive in terms of computational cost by comparing them against LAMMPS’s Ewald and P3M implementations using the same replicated crystal structures shown in Figure 3. The LAMMPS benchmarks are performed using the version from August 2, 2023 (Update 3), in combination with the Kokkos 4.3.1 package. For our Ewald and P3M benchmarks, we used the same parameters optimized by LAMMPS for a relative force accuracy of  $10^{-4}$ . For PME, we utilize our own tuning code, aiming for an absolute force accuracy of  $10^{-4}$ . In all cases, we employed a fixed cutoff of  $4.4 \text{ \AA}$ , which provided the best performance for our largest structure, containing approximately 263,000 atoms in a cubic cell with a side length of  $65 \text{ \AA}$ . See Figure S3 for a visualization of the grid search used to determine this cutoff value. All reported timings include only the evaluation of the short- and long-range components of the Coulomb potential, as well as its derivatives. Notably, they do not account for the computation of the neighbor list. This exclusion is justified because, in typical machine learning applications, the long-range part of the architecture is often combined with a short-range one, where the neighbor list can usually be reused. Additionally, in MD applications, the neighbor list can be reused for multiple timesteps.

Figure 4 shows that for small system sizes up to about  $N = 1000$  atoms, LAMMPS Ewald (Figure 4A) is the fastest implementation, followed by the PME method in *jax-pme* and then *torch-pme*. We can see that the cost for our implementation is more or less constant across this range, meaning that this is not due to an inefficiency in the actual algorithm, but rather a general overhead required during the initialization. Even though these overheads are hard-to-quantify, probably they are related to a better CUDA kernel initialization and dispatch on the

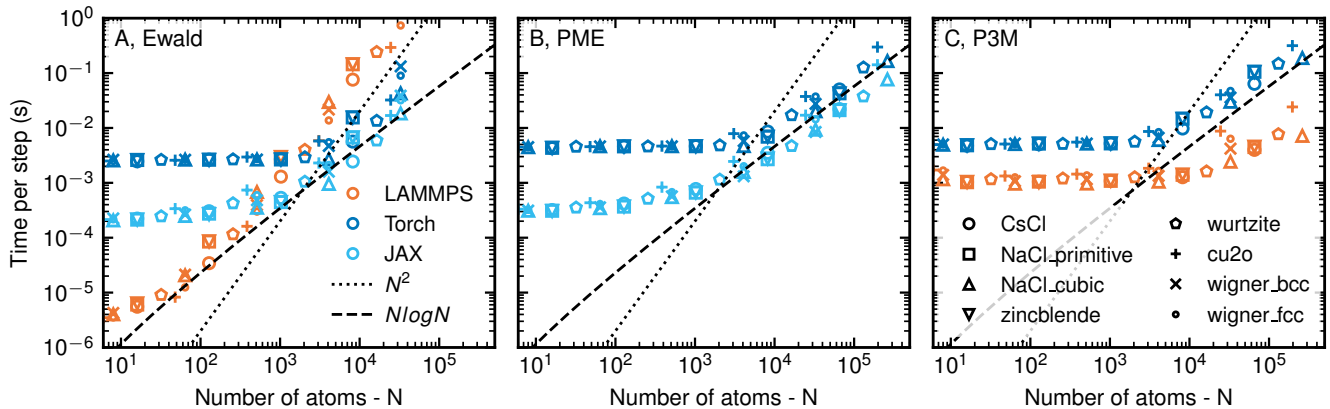


Figure 4. Benchmark for computational cost of long-range calculators to run a single point evaluation of the energy, force and stress for different replicated crystal structures. Panels show results for Ewald (A) PME (B) and P3M (C). Different crystals are shown as different symbols. Each point is an average of 50 single point calculations of the same positions with a tuning accuracy of  $1 \cdot 10^{-4}$ .

GPU by *JAX*. After a transition region between  $N = 10^3$  and  $N = 10^4$ , we observe that our Ewald implementations outperform the LAMMPS one, while all codes show the expected scaling of  $\mathcal{O}(N^2)^{34}$ . The mesh-based algorithms are competitive with the LAMMPS P3M implementation, while also showing the correct scaling of  $\mathcal{O}(N \log N)^{34}$ . For a system size of  $N = 10^4$ , the mesh-based algorithms are already faster than the Ewald ones by a factor of about 5, with the gap widening quickly due to the  $\mathcal{O}(N^2)$  asymptotic scaling of the latter. From these observations, we conclude that the implementations are fast enough for most practical applications and further recommend using the Ewald codes during the training step, as it usually involves small structures and is up to an order of magnitude faster compared to PME. After training, and when running production simulations, one should switch to the PME or P3M calculators to achieve the best performance for larger systems. Note that switching between the two calculators is unproblematic as both can be tuned to achieve high, and consistent, accuracy as demonstrated in Figure 3, and provide a drop-in replacement with fully compatible APIs.

## B. Molecular Dynamics

Even though *torch-pme* is designed with ML applications in mind, it is a good sanity check to verify it can be used as an empirical forcefield engine. To this end, we build a model that evaluates the electrostatic contributions for a SPC/E water model, and use the Metatensor framework<sup>71</sup> to export a *Torchscript* model that can be loaded and executed within the LAMMPS simulation engine<sup>72</sup>. We then perform a 2 ns NpT simulation of  $N = 256$  rigid water molecules. The time step of the simulation is set to 2 fs and the positions are recorded every 200 steps (0.2 ps). Temperature is controlled using

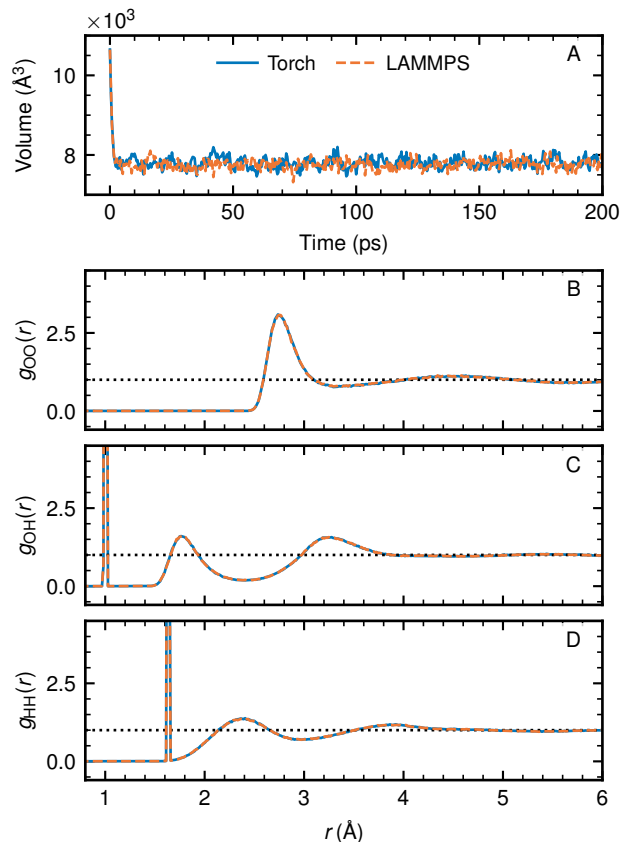


Figure 5. A: Time series of the first 200 ps showing the fluctuating volume of an NpT simulation of rigid SPC/E water. The Coulombic part of the interactions are either handled our PME (blue) or LAMMPS's own P3M implementation (red). B – D: Oxygen-oxygen  $g_{OO}$ , oxygen-hydrogen  $g_{OH}$  and hydrogen-hydrogen  $g_{HH}$  radial distribution functions.

the CSVR thermostat<sup>73</sup> and the pressure using a Nosé-Hoover barostat. During the simulation the Coulomb interaction between the particles was either handled by LAMMPS or the *torch-pme* implementation, both tuned to achieve a target accuracy of  $\epsilon = 10^{-6}$ . Note that any of the grid-based implementations could also be used, but our benchmarks show that, since the number of atoms is still small ( $N < 1000$ ), the Ewald implementation is faster. All other interaction such as Lennard-Jones were handled using the LAMMPS package. In Figure 5 (a) we show the time evolution of the system volume, in which the cell equilibrates from the initial configuration (a cubic cell with a side of 22 Å), reaching the same equilibrium volume. From the volume fluctuations we can compute the isothermal compressibility

$$\kappa_T = -\frac{1}{V} \left. \frac{\partial V}{\partial p} \right|_T. \quad (29)$$

The literature value for SPC/E water is  $\kappa_{T,\text{ref}} = 4.61 \cdot 10^{-10} \text{ m}^2\text{N}^{-1}$ <sup>74</sup> which agrees well with our obtained result of  $\kappa_T = (4.6 \pm 0.3) \cdot 10^{-10} \text{ m}^2\text{N}^{-1}$  and for LAMMPS  $\kappa_{T,\text{LAMMPS}} = (4.9 \pm 0.2) \cdot 10^{-10} \text{ m}^2\text{N}^{-1}$ . We obtain our values by leaving out the first 10 ps of the simulation for equilibration and calculate the error by an block average using 10 blocks. In Figure 5 (b) to (d), we show the radial distribution function between the two methods which are essentially identical.

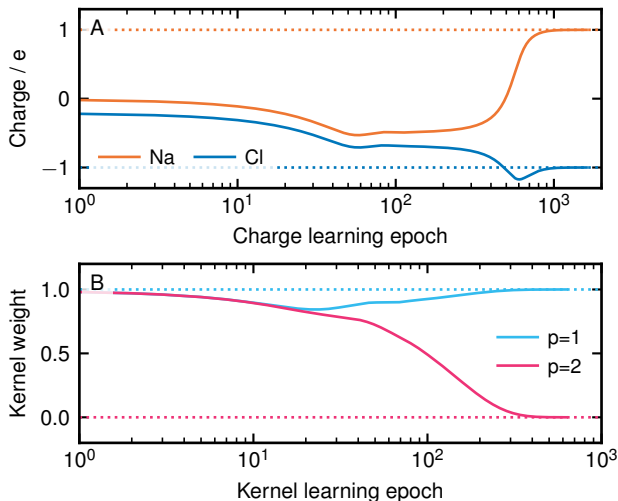


Figure 6. Learning curve for the charge of the sodium and chloride atoms optimized on the energy 10 random structures (A) and for optimizing the prefactor of two Fourier space kernels with different exponents  $p$  (B).

### C. Learning charges and potentials

To illustrate how to use *torch-pme* as a flexible module for machine learning tasks, we design two toy examples

that demonstrate the the possibility of optimizing atomic pseudo-charges, and the functional form of the pair interactions. For both, we use a dataset of 1000 NaCl structures each consisting of  $N = 64$  randomly placed atoms in cubic boxes of various side lengths that was already used in previous work<sup>59,61</sup>. Half of the atoms are Na atoms and assigned a fixed charged of  $q_{\text{Na}} = +1$ , while the other half are Cl atoms with a charge of  $q_{\text{Cl}} = -1$ . The total energy and forces of the systems are then computed assuming a pure Coulomb interaction between the atoms with an external reference calculator.

In both of the models that we will now discuss, the optimization was performed using the Adam optimizer with a maximum learning rate of  $1 \cdot 10^{-2}$  as implemented in *PyTorch*. In the first model, we make the atomic charges  $q_{\text{Na}}$  and  $q_{\text{Cl}}$  learnable parameters, and initialize them to a small but nonzero value. Note that we do not explicitly enforce charge neutrality, even though it could help for more complex systems. The two charges are then optimized by fitting on the energy of the structures. Figure 6 (a) shows the charges as a function of the number of epochs in the training procedure. We can see that even though the convergence is not monotonic, the charges reach the correct values after about 1000 epochs.

In the second model, we fix  $q_{\text{Na}} = +1$  and  $q_{\text{Cl}} = -1$  but this time modify the interaction potential to be of the form

$$v(r) = \frac{w_1}{r} + \frac{w_2}{r^2}, \quad (30)$$

with learnable weights  $w_1$  and  $w_2$ . Figure 6 (b) shows the evolution of these weights, again as a function of the number of epochs. We can see that after about 1000 epochs, both weights converge to the expected, reference values of  $w_1 = 1$  and  $w_2 = 0$ .

Example files that were used to run these calculations are provided as examples in the package repositories and documentation. They demonstrate the flexibility to effortlessly optimize various intermediate parameters that appear during calculations.

### D. A model with learnable local charges

To demonstrate a more realistic application, we developed a complete end-to-end machine learning model and evaluated its performance on the organic molecules dataset developed in our previous work Ref 61 as shown in Figure 7A. The model has the overall structure of a “third-generation” neural network potential<sup>75</sup>. It predicts the potential energy of a system, which we decompose into atom-wise energy contributions:  $E_{\text{system}} = \sum_{i=1}^N E_i$ , where  $E_{\text{system}}$  is the total potential energy of the system,  $N$  is the number of atoms, and  $E_i$  represents the energy contribution from a single atom. We further decompose the atom-wise energy into short-range (SR) and long-range (LR) components:  $E_i = E_{\text{SR},i} + E_{\text{LR},i}$ . The SR part is computed using an atomic Neural Network (NN) which takes as input an invariant descriptor

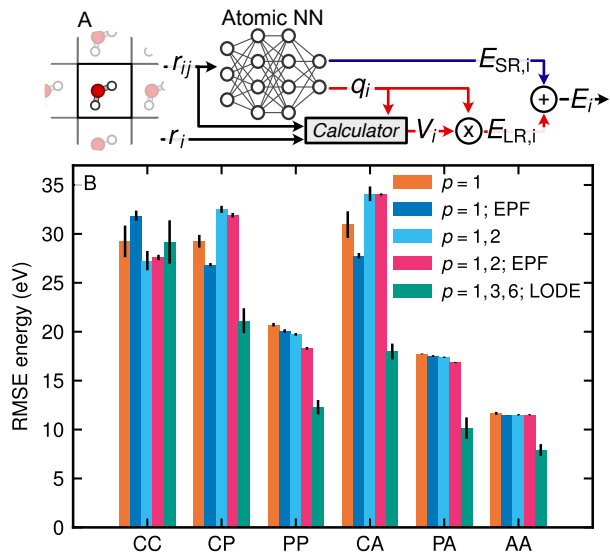


Figure 7. Schematic representation of an architecture that combines an atomic NN with a range separated calculator (A) and bar plots showing the comparison of RMSE on energies for different test subsets (B): charge-charge (CC), charge-polar (CP), polar-polar (PP), charge-apolar (CA), polar-apolar (PA), apolar-apolar (AA). Orange bars represent results from the architectures taken from Ref. 61 while all other bars represent results from the architecture described in panel (A).

representing the local atomic environment within a pre-defined cutoff radius  $r_{cut}$ :  $E_{SR,i} = F_{\theta}(w_i)$  where  $w_i$  is a vector describing the environment of atom  $i$ . For our implementation, we used the Smooth Overlap of Atomic Positions (SOAP)<sup>2</sup> parameterization with the same parameters as in Ref 61. The NN consists of three layers, each with 256 neurons. Training was conducted for 200 epochs using the Adam optimizer with the OneCycleLR policy<sup>76</sup> and a maximum learning rate of  $5 \cdot 10^{-4}$ . Besides predicting the  $E_{SR,i}$  the same model predicts also the atomic charges  $q_i = F_{\theta}^*(w_i)$ , which serve as inputs to a *torch-pme* Calculator to compute the long-range potential  $V_i$  and energy  $E_{LR,i} = q_i \cdot V_i$ . In Figure 7B, we show a comparison of the results obtained using our pipeline. Specifically, we consider four cases for  $V_i$ : (1) using the full Coulomb potential ( $p = 1$ ), (2) using the Coulomb EPFs ( $p = 1$ ; EPF), (3) using a linear combination of the Coulomb potential and a  $1/r^2$  term with learnable weights ( $p = 1, 2$ ), and (4) using linear combination of the Coulomb EPFs and a  $1/r^2$  term EPFs with learnable weights ( $p = 1, 2$ , EPF). We compare the obtained results to those from Ref. 61, where LODE descriptors were employed which includes on the order of  $10^3$  features per atom, whereas our current pipeline generates only a single descriptor. We find that we achieve similar accuracy for the charge-charge partitioning, which is the dominating contribution in the dataset. However, we tend to perform slightly worse on other partitions, as

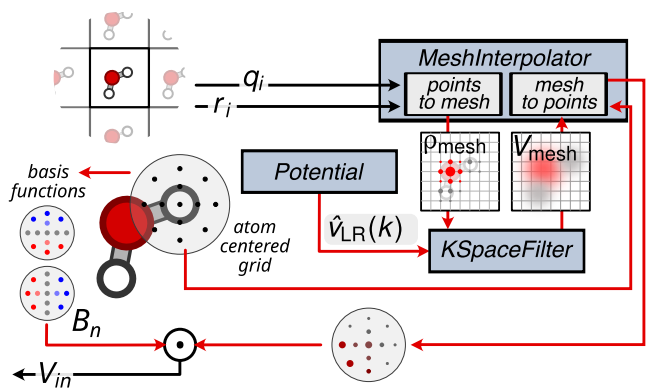


Figure 8. A schematic representation of the architecture of a model that computes LODE features, by evaluating the long-range part of the potential on a real-space grid, interpolating it on atom-centered grids, and combining it with a set of basis functions to evaluate atom-centered descriptors  $V_{in}$ , that are rotationally equivariant as long as the chosen basis functions are.

these are no longer dominated by simple Coulomb-like interactions. This discrepancy is unsurprising because the LODE descriptors use more features to capture appearing long-range interactions beside the Coulombic ones. Similar to what was observed in Ref. 61, the inclusion of an additional exponent (e.g.,  $p = 2$  in our case) does not yield better results. This finding indicates that, for the studied dataset, the most significant contribution to the long-range energetics is provided by electrostatic terms. Combined with learnable charges, a single descriptor restricted to long-range information is sufficient to capture the most prominent energetic contributions. Finally, we observe that using EPFs provides only a marginal improvement in most cases (except for the charge-charge pair, where a decrease in accuracy is expected due to the EPFs breaking strict physical description). For this simple model and small dataset, the fact that  $E_{LR}$  contains a short-range contribution can be compensated by the flexibility of  $E_{SR}$ . A clear-cut range separation is still very useful – e.g. to accelerate the evaluation of the model with multiple time stepping – and it may prove beneficial in more complex models, or when used for long-range effects that are not dominated by electrostatics.

## E. Long distance equivariant features

As an example of how modular design and automatic differentiation help adapt classical algorithms for long-range interactions to modern machine learning tasks, we discuss how to evaluate long-distance equivariant (LODE) features. The basic idea behind LODE<sup>59</sup>, and its generalization to  $1/r^p$  potentials<sup>61</sup>, is to first compute the potential  $V(\mathbf{r}) = \sum_i q_i v(|\mathbf{r} - \mathbf{r}_i|)$ , generated by the atoms with weights  $q_i$ , and then to expand it in an

atom-centered basis

$$V_{in} = \int V(\mathbf{r})B_n(\mathbf{r} - \mathbf{r}_i) d\mathbf{r}, \quad (31)$$

where  $B_n$  are a set of basis functions. Usually, the basis functions are factorized in radial functions and spherical harmonics, but this is inconsequential from the point of view of the implementation (see Fig. 8).

The first step involves computing  $V(\mathbf{r})$  on a real-space grid. This can be achieved with a Fourier convolution, exactly as in a grid-based long-range calculator. A subtlety is that it is less convenient to include a short-range correction, because one would have to evaluate it at all grid points, and not only at atomic positions, requiring one to build an additional neighbor list and to compute a much larger number of real-space pair interactions. Alternatively, and given that the objective is to build long-range *descriptors* rather than to compute a precise physical interaction, one can use exclusively  $v_{LR}$  and compute only the reciprocal space component. If one wants to do this while also subtracting the interior contribution, the cutoff function has to be included in the computation of  $\hat{v}_{LR}$ ; given that this cannot be done analytically for a general, smooth cutoff function, we implement a potential based on real-space cubic splines, which is numerically processed to generate the Fourier kernel.

After having obtained  $V(\mathbf{r})$  on a regular mesh, we have to evaluate the integral (31). To do so, one can define an atom-centered mesh within a ball with the desired radius, and interpolate the potential at the grid points. Then, the integral can be performed as a dot product with the basis function, pre-computed on the same grid, and appropriate quadrature weights. Given that the *MeshInterpolator* class allows interpolating on arbitrary points, this architecture can be realized very easily, and the resulting method is quite fast given also the the basis functions are pre-computed at initialization, competitive with the existing implementations of LODE<sup>77</sup> also for systems of moderate size.

## V. CONCLUSION

We have presented a highly flexible framework to perform long-range ML efficiently, and provide two reference implementations in *PyTorch* and *JAX*. Our method allows us to compute not only electrostatic and more general inverse power-law potentials of the form  $1/r^p$ , but also to produce purified descriptors that exclusively contain information about atoms outside of the cutoff radius. This is useful when combining these features with short-range ML models, and can be used to predict any invariant or equivariant target property. The features can be computed using a variety of methods: Ewald summation is well-suited for small to moderate system sizes with hundreds of atoms, while the particle-mesh algorithms such as PME and P3M scale almost linearly with

system size,  $\mathcal{O}(N \log N)$ , and are hence well-suited for larger structures.

Our reference implementation fully exploit the flexibility and automatic differentiation capabilities of the *PyTorch* and *JAX* libraries, allowing for smooth integration into any preexisting ML architecture. The ML capabilities of the libraries is also used to automatically optimize hyperparameters, further streamlining ease of use, with benchmarks confirming the competitive speed and accuracy of the implementations. Besides the direct application to improve existing short-range models our implementations also allow an easier inclusion of applied external potentials or fields into machine learning models<sup>11,78</sup>. The modular structure also allows for various modifications for power-users who wish to fully exploit the flexibility of the implementations. We hope that the availability of these libraries will encourage the development of more standardized, efficient and scalable long-range ML models, and that their modular design will allow to develop more flexible, general models than the simple point-charge examples we discuss here.

## VI. SUPPLEMENTARY MATERIAL

The electronic supporting material for this publication include further details on the implementation, different models and datasets, and additional results on benchmarks. The source code *torch-pme* and *jax-pme* packages are publicly available at <https://github.com/lab-cosmo/torch-pme> and <https://github.com/lab-cosmo/jax-pme>. Some results are compared with the generalized LODE descriptors introduced in previous work by the authors, which have been computed using the *featomic* (formerly *rascaline*) package<sup>77</sup>, available at <https://github.com/metatensor/featomic>.

## ACKNOWLEDGMENTS

MC, KKHD, MFL, PL and WBH acknowledge funding from the European Research Council (ERC) under the research and innovation programme (Grant Agreement No. 101001890-FIAMMA). MC, PL, ER and MH acknowledge funding from the NCCR MARVEL, funded by the Swiss National Science Foundation (SNSF, grant number 182892), which also supported a research internship for MH through an Inspire Potentials Fellowship. We would like to thank the members of the Laboratory of Computational Science and Modeling, and especially Guillaume Fraux, Filippo Bigi and Arslan Mazitov, for their contributions to the software infrastructure that enabled this study. We further thank Philipp Stärk for the discussions.

## DATA AVAILABILITY STATEMENT

The source code to our *PyTorch* and *JAX* libraries are available on Github at <https://github.com/lab-cosmo/torch-pme> and <https://github.com/lab-cosmo/jax-pme>. Code to reproduce Figure 6 as well as how to construct LODE densities are available as tutorials in the *torch-pme* documentation. All other codes and input files for computing the accuracies, running benchmarks, MD simulations, and the model with learnable local charges are as well available on Github at <https://github.com/PicoCentauri/ewaldAD-code>.

## REFERENCES

- J. Behler and M. Parrinello, "Generalized neural-network representation of high-dimensional potential-energy surfaces," *Physical Review Letters* **98**, 146401 (2007).
- A. P. Bartók, M. C. Payne, R. Kondor, and G. Csányi, "Gaussian approximation potentials: The accuracy of quantum mechanics, without the electrons," *Physical Review Letters* **104**, 136403 (2010).
- M. Rupp, A. Tkatchenko, K.-R. Müller, and O. A. von Lilienfeld, "Fast and accurate modeling of molecular atomization energies with machine learning," *Physical Review Letters* **108**, 058301 (2012).
- K. T. Schütt, H. E. Sauceda, P.-J. Kindermans, A. Tkatchenko, and K.-R. Müller, "Schnet – a deep learning architecture for molecules and materials," *The Journal of Chemical Physics* **148**, 241722 (2018).
- K. T. Schütt, P.-J. Kindermans, H. E. Sauceda, S. Chmiela, A. Tkatchenko, and K.-R. Müller, "Schnet: A continuous-filter convolutional neural network for modeling quantum interactions," *Advances in Neural Information Processing Systems* **30** (2017).
- J. Klicpera, S. Giri, J. T. Margraf, and S. Günnemann, "Directional message passing for molecular graphs," *International Conference on Learning Representations* (2020).
- L. Zhang, J. Han, H. Wang, R. Car, and W. E, "Deep potential molecular dynamics: A scalable model with the accuracy of quantum mechanics at the cost of classical molecular dynamics," *Physical Review Letters* **120**, 143001 (2018).
- N. Thomas, T. E. Smidt, S. Kearnes, L. Yang, L. Li, K. Kohlhoff, and P. Riley, "Tensor field networks: Rotation- and translation-equivariant neural networks for 3d point clouds," *arXiv preprint arXiv:1802.08219* (2018).
- A. Musaelian, S. Batzner, A. Johansson, L. Sun, C. J. Owen, M. Kornbluth, and B. Kozinsky, "Learning local equivariant representations for large-scale atomistic dynamics," *Nat Commun* **14**, 579 (2023).
- A. Glielmo, P. Sollich, and A. De Vita, "Accurate interatomic force fields via machine learning with covariant kernels," *Physical Review B* **95**, 214302 (2017).
- A. Grisafi, D. M. Wilkins, G. Csányi, and M. Ceriotti, "Symmetry-adapted machine learning for tensorial properties of atomistic systems," *Physical Review Letters* **120**, 036002 (2018).
- D. M. Wilkins, A. Grisafi, Y. Yang, K. U. Lao, R. A. DiStasio Jr., and M. Ceriotti, "Accurate molecular polarizabilities with coupled cluster theory and machine learning," *Proceedings of the National Academy of Sciences* **116**, 3401–3406 (2019).
- F. Brockherde, L. Vogt, L. Li, M. E. Tuckerman, K. Burke, and K.-R. Müller, "Bypassing the kohn-sham equations with machine learning," *Nature Communications* **8**, 872 (2017).
- A. Fabrizio, A. Grisafi, B. Meyer, and C. Corminboeuf, "Electron density learning of non-covalent systems," *Chemical Science* **10**, 9424–9432 (2019).
- A. J. Lewis, A. Grisafi, M. Ceriotti, and M. Rossi, "Learning electron density in the condensed phase," *Journal of Chemical Theory and Computation* **17**, 6725–6737 (2021).
- K. T. Schütt, M. Gastegger, A. Tkatchenko, K.-R. Müller, and R. J. Maurer, "Unifying machine learning and quantum chemistry with a deep neural network for molecular wavefunctions," *Nature Communications* **10**, 5024 (2019).
- E. Cignoni, D. Suman, J. Nigam, L. Cupellini, B. Menzies, and M. Ceriotti, "Electronic excited states from physically constrained machine learning," *ACS Central Science* **10**, 637–648 (2024), <https://doi.org/10.1021/acscentsci.3c01480>.
- G. Carleo and M. Troyer, "Solving the quantum many-body problem with artificial neural networks," *Science* **355**, 602–606 (2017).
- J. Hermann, Z. Schätzle, and F. Noé, "Deep-neural-network solution of the electronic schrödinger equation," *Nature Chemistry* **12**, 891–897 (2020).
- O. T. Unke, M. Bogojeski, M. Gastegger, M. Geiger, T. Smidt, and K.-R. Müller, "SE(3)-equivariant prediction of molecular wavefunctions and electronic densities," (2021), [arXiv:2106.02347](https://arxiv.org/abs/2106.02347).
- W. Fulton and J. Harris, *Representation Theory: A First Course*, Graduate Texts in Mathematics, Vol. 129 (Springer-Verlag, New York, 1991).
- J.-P. Serre, *Linear Representations of Finite Groups*, Graduate Texts in Mathematics, Vol. 42 (Springer-Verlag, New York, 1977).
- M. Tinkham, *Group Theory and Quantum Mechanics* (Dover Publications, Mineola, NY, 2003) originally published in 1964 by McGraw-Hill.
- W. Kohn, "Density functional and density matrix method scaling linearly with the number of atoms," *Phys. Rev. Lett.* **76**, 3168–3171 (1996).
- E. Prodan and W. Kohn, "Nearsightedness of electronic matter," *Proceedings of the National Academy of Sciences* **102**, 11635–11638 (2005), <https://www.pnas.org/content/102/33/11635.full.pdf>.
- C. J. Fennell and J. D. Gezelter, "Is the ewald summation still necessary? pairwise alternatives to the accepted standard for long-range electrostatics," *Journal of Chemical Physics* **124**, 234104 (2006).
- M. Born and K. Huang, "Dynamical theory of crystal lattices," Oxford University Press (1954).
- J. D. Jackson, *Classical Electrodynamics Third Edition*, 3rd ed. (Wiley, New York, 1998).
- S. Grimme, "Semiempirical gga-type density functional constructed with a long-range dispersion correction," *Journal of Computational Chemistry* **27**, 1787–1799 (2006).
- A. Tkatchenko and M. Scheffler, "Accurate molecular van der waals interactions from ground-state electron density and free-atom reference data," *Physical Review Letters* **102**, 073005 (2009).
- R. A. DiStasio, V. V. Gobre, and A. Tkatchenko, "Many-body van der waals interactions in molecules and condensed matter," *Journal of Physics: Condensed Matter* **26**, 213202 (2014).
- J. M. Borwein, M. L. Glasser, R. C. McPhedran, J. G. Wan, and I. J. Zucker, *Lattice Sums Then and Now*, Encyclopedia of Mathematics and its Applications (Cambridge University Press, 2013).
- P. P. Ewald, "Die Berechnung optischer und elektrostatischer Gitterpotentiale," *Annalen der Physik* **369**, 253–287 (1921).
- M. P. Allen and D. J. Tildesley, *Computer Simulation of Liquids* (Oxford University Press, 2017).
- B. R. A. Nijboer and F. W. De Wette, "On the calculation of lattice sums," *Physica* **23**, 309–321 (1957).
- D. E. Williams, "Accelerated convergence of crystal-lattice potential sums," *Acta Crystallographica Section A* **27**, 452–455 (1971).
- D. E. Williams, "Accelerated Convergence Treatment of R-n Lattice Sums," *Crystallography Reviews*

- 2, 3–23 (1989), publisher: Taylor & Francis eprint: <https://doi.org/10.1080/08893118908032944>.
- <sup>38</sup>N. Karasawa and W. A. Goddard III, “Acceleration of convergence for lattice sums,” *The Journal of Physical Chemistry* **93**, 7320–7327 (1989).
- <sup>39</sup>R. W. Hockney and J. W. Eastwood, “Computer simulation using particles,” CRC Press (1981).
- <sup>40</sup>M. Deserno and C. Holm, “How to mesh up Ewald sums. I. A theoretical and numerical comparison of various particle mesh routines,” *J. Chem. Phys.* **109**, 7678–7693 (1998).
- <sup>41</sup>T. Darden, D. York, and L. Pedersen, “Particle mesh ewald: An n-log(n) method for ewald sums in large systems,” *Journal of Chemical Physics* **98**, 10089–10092 (1993).
- <sup>42</sup>U. Essmann, L. Perera, M. L. Berkowitz, T. Darden, H. Lee, and L. G. Pedersen, “A smooth particle mesh ewald method,” *The Journal of chemical physics* **103**, 8577–8593 (1995).
- <sup>43</sup>W. Gautschi, *Numerical analysis* (Springer Science & Business Media, 2011).
- <sup>44</sup>L. Greengard and V. Rokhlin, “A fast algorithm for particle simulations,” *Journal of Computational Physics* **73**, 325–348 (1987).
- <sup>45</sup>P. Gibbon and G. Sutmann, “Long-range interactions in many-particle simulation,” *Quantum Simulations of Complex Many-Body Systems: From Theory to Algorithms*, NIC Series , 467–506 (2004).
- <sup>46</sup>Z. Deng, C. Chen, X.-G. Li, and S. P. Ong, “An electrostatic spectral neighbor analysis potential for lithium nitride,” *npj Computational Materials* **5**, 1–8 (2019).
- <sup>47</sup>V. L. Deringer, M. A. Caro, and G. Csányi, “A general-purpose machine-learning force field for bulk and nanostructured phosphorus,” *Nat Commun* **11**, 5461 (2020).
- <sup>48</sup>O. T. Unke, S. Chmiela, M. Gastegger, K. T. Schütt, H. E. Sauceda, and K.-R. Müller, “Spookynet: Learning force fields with electronic degrees of freedom and nonlocal effects,” *Nature communications* **12**, 7273 (2021).
- <sup>49</sup>S. P. Niblett, M. Galib, and D. T. Limmer, “Learning intermolecular forces at liquid–vapor interfaces,” *J. Chem. Phys.* **155**, 164101 (2021).
- <sup>50</sup>A. Kabylda, J. T. Frank, S. S. Dou, A. Khabibrakhmanov, L. M. Sandonas, O. T. Unke, S. Chmiela, K.-R. Müller, and A. Tkatchenko, “Molecular simulations with a pretrained neural network and universal pairwise force fields,” *chemrxiv preprint* (2024), 10.26434/chemrxiv-2024-bdf0.
- <sup>51</sup>O. T. Unke and M. Meuwly, “Physnet: A neural network for predicting energies, forces, dipole moments, and partial charges,” *Journal of Chemical Theory and Computation* **15**, 3678–3693 (2019), pMID: 31042390, <https://doi.org/10.1021/acs.jctc.9b00181>.
- <sup>52</sup>A. E. Sifain, N. Lubbers, B. T. Nebgen, J. S. Smith, A. Y. Lokhov, O. Isayev, A. E. Roitberg, K. Barros, and S. Tretiak, “Discovering a transferable charge assignment model using machine learning,” *The Journal of Physical Chemistry Letters* **9**, 4495–4501 (2018), pMID: 30039707, <https://doi.org/10.1021/acs.jpcltt.8b01939>.
- <sup>53</sup>Y. Peng, L. Lin, L. Ying, and L. Zepeda-Núñez, “Efficient long-range convolutions for point clouds,” *Journal of Computational Physics* **473**, 111692 (2023).
- <sup>54</sup>L. Zhang, H. Wang, M. C. Muniz, A. Z. Panagiotopoulos, R. Car, and W. E, “A deep potential model with long-range electrostatic interactions,” *J. Chem. Phys.* **156**, 124107 (2022).
- <sup>55</sup>S. Faraji, S. A. Ghasemi, S. Rostami, R. Rasoulkhani, B. Schaefer, S. Goedecker, and M. Amsler, “High accuracy and transferability of a neural network potential through charge equilibration for calcium fluoride,” *Phys. Rev. B* **95**, 104105 (2017).
- <sup>56</sup>T. W. Ko, J. A. Finkler, S. Goedecker, and J. Behler, “A fourth-generation high-dimensional neural network potential with accurate electrostatics including non-local charge transfer,” *Nat Commun* **12**, 398 (2021).
- <sup>57</sup>T. W. Ko, J. A. Finkler, S. Goedecker, and J. Behler, “General-Purpose Machine Learning Potentials Capturing Non-local Charge Transfer,” *Acc. Chem. Res.* **54**, 808–817 (2021).
- <sup>58</sup>M. Gubler, J. A. Finkler, M. R. Schäfer, J. Behler, and S. Goedecker, “Accelerating Fourth-Generation Machine Learning Potentials Using Quasi-Linear Scaling Particle Mesh Charge Equilibration,” *J. Chem. Theory Comput.* (2024), 10.1021/acs.jctc.4c00334.
- <sup>59</sup>A. Grisafi and M. Ceriotti, “Incorporating long-range physics in atomic-scale machine learning,” *J. Chem. Phys.* **151**, 204105 (2019).
- <sup>60</sup>A. Grisafi, J. Nigam, and M. Ceriotti, “Multi-scale approach for the prediction of atomic scale properties,” *Chem. Sci.* **12**, 2078–2090 (2021).
- <sup>61</sup>K. K. Huguenin-Dumittan, P. Loche, N. Haoran, and M. Ceriotti, “Physics-Inspired Equivariant Descriptors of Nonbonded Interactions,” *J. Phys. Chem. Lett.* , 9612–9618 (2023).
- <sup>62</sup>S. Chong, F. Bigi, F. Grasselli, P. Loche, M. Kellner, and M. Ceriotti, “Prediction rigidities for data-driven chemistry,” *Faraday Discussions* (2024), 10.1039/D4FD00101J.
- <sup>63</sup>B. Cheng, “Latent Ewald summation for machine learning of long-range interactions,” (2024), arXiv:2408.15165.
- <sup>64</sup>C. Faller, M. Kaltak, and G. Kresse, “Density-Based Long-Range Electrostatic Descriptors for Machine Learning Force Fields,” (2024), arXiv:2406.17595.
- <sup>65</sup>G. Hummer, “The numerical accuracy of truncated ewald sums for periodic systems with long-range coulomb interactions,” *Chemical Physics Letters* **235**, 297–302 (1995).
- <sup>66</sup>H. G. Petersen, “Accuracy and efficiency of the particle mesh Ewald method,” *The Journal of Chemical Physics* **103**, 3668–3679 (1995).
- <sup>67</sup>M. E. Tuckerman, B. J. Berne, and A. Rossi, “Molecular dynamics algorithm for multiple time scales: Systems with disparate masses,” *The Journal of Chemical Physics* **94**, 1465–1469 (1991).
- <sup>68</sup>V. Kapil, J. VandeVondele, and M. Ceriotti, “Accurate molecular dynamics and nuclear quantum effects at low cost by multiple steps in real and imaginary time: Using density functional theory to accelerate wavefunction methods,” *The Journal of Chemical Physics* **144**, 054111 (2016).
- <sup>69</sup>J. E. House, “Chapter 7 - Ionic bonding and structures of solids,” in *Inorganic Chemistry (Third Edition)*, edited by J. E. House (Academic Press, 2020) pp. 229–274.
- <sup>70</sup>L. Glasser, “Solid-State Energetics and Electrostatics: Madelung Constants and Madelung Energies,” *Inorg. Chem.* **51**, 2420–2424 (2012).
- <sup>71</sup>G. Fraux, P. Loche, F. Bigi, J. W. Abbott, D. Tisi, A. Goscinski, and M. Ceriotti, “Metatensor,” (2024).
- <sup>72</sup>A. P. Thompson, H. M. Aktulga, R. Berger, D. S. Bolintineanu, W. M. Brown, P. S. Crozier, P. J. in ’t Veld, A. Kohlmeyer, S. G. Moore, T. D. Nguyen, R. Shan, M. J. Stevens, J. Tranchida, C. Trott, and S. J. Plimpton, “LAMMPS - a flexible simulation tool for particle-based materials modeling at the atomic, meso, and continuum scales,” *Computer Physics Communications* **271**, 108171 (2022).
- <sup>73</sup>G. Bussi, D. Donadio, and M. Parrinello, “Canonical sampling through velocity rescaling,” *The Journal of Chemical Physics* **126**, 014101 (2007).
- <sup>74</sup>C. Vega and J. L. F. Abascal, “Simulating water with rigid non-polarizable models: A general perspective,” *Phys. Chem. Chem. Phys.* **13**, 19663–19688 (2011).
- <sup>75</sup>J. Behler, “Four Generations of High-Dimensional Neural Network Potentials,” *Chemical Reviews* **121**, 10037–10072 (2021).
- <sup>76</sup>L. N. Smith and N. Topin, “Super-convergence: Very fast training of neural networks using large learning rates,” in *Artificial intelligence and machine learning for multi-domain operations applications*, Vol. 11006 (SPIE, 2019) pp. 369–386.
- <sup>77</sup>G. Fraux, P. Loche, F. Bigi, J. W. Abbott, L. Marsh, S. Klavinek, A. Goscinski, K. K. Huguenin-Dumittan, D. Suman, R. K. Cersonsky, and D. Tisi, “featomic,” (2024).
- <sup>78</sup>L. J. V. Ahrens-Iwers and R. H. Meißner, “Constant potential simulations on a mesh,” *The Journal of Chemical Physics* **155**, 104104 (2021).